Wear 572-573 (2025) 206041

Contents lists available at ScienceDirect

Wear

journal homepage: www.elsevier.com/locate/wear

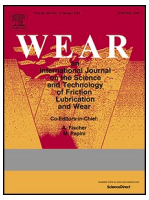

Tribological improvement using $Ti_3C_2T_x$ MXenes and/or $CaCO_3$ nanoparticles as lubricant additives

José M. Liñeira del Río [a,*], Martín Gómez Martínez [a], Antonio Moreda-Piñeiro [b], Enriqueta R. López [a], Josefa Fernández [a]

[a] Laboratory of Thermophysical and Tribological Properties, Nafomat Group, Department of Applied Physics, Faculty of Physics, and Institute of Materials (iMATUS), Universidade de Santiago de Compostela, 15782, Santiago de Compostela, Spain
[b] Trace Element, Spectroscopy and Speciation Group (GETEE), Institute of Materials iMATUS, Department of Analytical Chemistry, Nutrition and Bromatology, Faculty of Chemistry, Universidade de Santiago de Compostela, Avenida das Ciencias, s/n, 15782, Santiago de Compostela, Spain

ARTICLE INFO

Keywords:
MXenes
Nanoparticles
Wear
Surface analysis

ABSTRACT

The main goal of this work is the tribological characterization of low viscosity nanolubricants, PAO8 base oil containing $Ti_3C_2T_x$ MXenes and/or functionalized $CaCO_3$ ($CaCO_3$-OA) nanoparticles as additives. Friction enhancements were reached with $CaCO_3$-OA nanolubricants with maximum reductions of 44 % for the optimal concentration of 0.10 wt% $CaCO_3$-OA. With respect to wear, significant improvements in antiwear performance were achieved with maximum reductions in wear width of 27 % (0.15 wt% $CaCO_3$-OA), 14 % (0.10 wt% $Ti_3C_2T_x$) and 13 % for hybrid (0.10 wt% $CaCO_3$-OA/$Ti_3C_2T_x$) nanolubricants. Confocal Raman microscopy was utilized to recognize the mechanisms that govern tribological improvement: tribofilm formation for $Ti_3C_2T_x$ nanosheets and tribofilm formation and self-repairing for $CaCO_3$-OA nanoparticles.

1. Introduction

In accordance with the continuous evolution of the automotive industry and the growing shift from vehicles with internal combustion engine (ICEVs) to hybrid and electric vehicles (EVs), transmission fluids must be modified to align with the distinct requirements of EVs [1]. The automotive industry is currently undergoing a transition towards the integration of e-modules, such as electrified powertrains. This fact demands the use of a single fluid, designated as the e-fluid, EV fluid, or electric transmission fluid (ETF), which is responsible for cooling the electrical windings of the motor and providing an optimal tribological efficiency under extreme conditions [2]. Low viscosity fluids are needed to enhance the cooling efficiency and have the advantage of providing significant energy reductions by decreasing viscous shear and pumping losses [2,3]. Gupta [4] estimated the effectiveness of an EV-modified Toyota Prius by using automatic transmission fluids (ATF) with diverse viscosities, finding that the greatest vehicle efficiency was reached with smallest viscosity oil (Lubrizol ATF, 45 cSt@40 °C). Currently, ATFs are frequently used in the electrified powertrains of EVs, even though the design of this e-module differs considerably from that of automatic transmissions [5]. The use of low-viscosity oils is a trend in the production of automotive lubricants and ETFs. However, in the case of ETFs, there are additional properties that must be considered in comparison with conventional engine or ATF lubricants. These include appropriate dielectric strength and electrical conductivity, high thermal conductivity, and good lubricity under high rotational speeds [2].

Polyalphaolefins (PAOs) are the most used base oils from synthetic nature, given their great tribological characteristics at high temperatures. Even with these advantageous characteristics, the incorporation of additives to improve their performance is needed. Especially in the case of ETFs as their viscosities must be very low and wear protection is critical. Currently, common ATFs and ETFs have kinematic viscosities at 100 °C in the range 6–8 cSt [5]. In the present era, a promising strategy for enhancing base oil tribological behavior is the incorporation of nanoparticles (NPs) as lubricant additives [6–9], reaching extraordinary improvements in friction and wear.

One advantage of utilizing NPs as additives of lubricant oils is their nanoscale dimensions, that facilitate their insertion into tribological contact and enable the development of an optimal lubrication effect [10]. In the case of two-dimensional (2D) layered nanomaterials, the weak van der Waals interaction between nanosheets provides low resistance to shear in the sliding direction under frictional stress, which

* Corresponding author.
E-mail address: josemanuel.lineira@usc.es (J.M. Liñeira del Río).

https://doi.org/10.1016/j.wear.2025.206041
Received 16 October 2024; Received in revised form 21 February 2025; Accepted 18 March 2025
Available online 19 March 2025

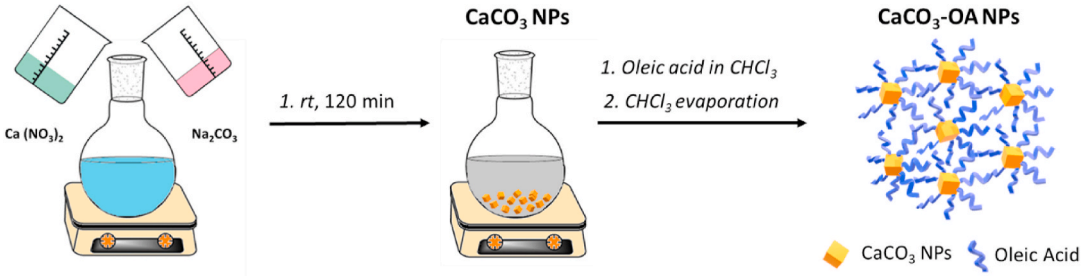

$$Na_2CO_{3(aq)} + Ca(NO_3)_{2(aq)} \rightarrow 2\ NaNO_{3(aq)} + CaCO_{3(s)}$$

Fig. 1. Scheme of the $CaCO_3$-OA nanoparticles synthesis.

$$LiF_{(s)} + HCl_{(aq)} \rightarrow LiCl_{(aq)} + HF_{(aq)}$$

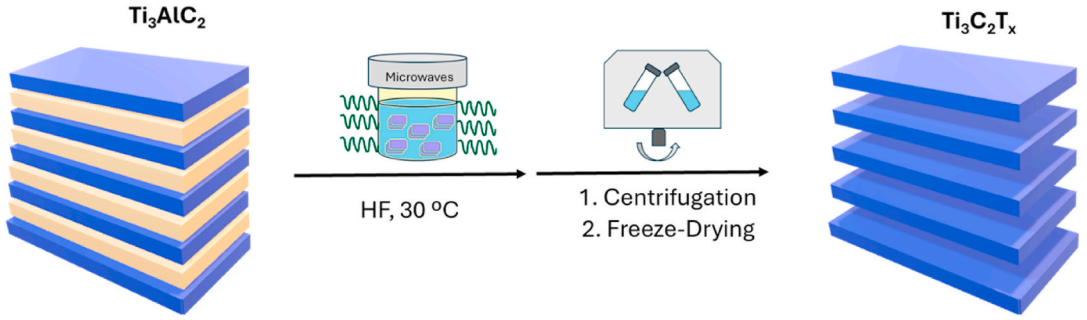

$$Ti_3AlC_{2\,(s)} + 3\ HF_{(aq)} \rightarrow Ti_3C_2T_{x\,(s)} + \frac{3}{2}H_{2\,(g)} + AlF_{3\,(aq)}$$

Fig. 2. Synthesis scheme of $Ti_3C_2T_x$ MXenes nanosheets.

Table 1
Test configuration and tribological settings as well as 3D Profilometer specifications.

Tribology Cell T-PTD200		
Disposition: Ball-on-three pins		
Pins and balls	Experimental characteristics	HPTD200
100Cr6 steel ball: 12.7 mm diameter and 0.15 μm Ra	Sample: 0.5 mL (3 repeats)	120 °C
100Cr6 pins: 3 mm radius and a 0.3 μm Ra	Load (F_N): 9.43 N (in each pin)	
For Pins and balls:	Max. contact pressure: 1 GPa	
Poisson ratio: 0.29; Hardness: 58–65 HRC; Young modulus: 190–210 GPa	Sliding Distance: 340 m Sliding speed: 0.10 m/s	
Profilometer S Neox (Sensofar)		
Characteristics	Quantified wear parameters	
Confocal mode 10 × Magnification objective SensoScan and SensoMap Software	Wear Scar Diameter (WSD) Wear Track Depth (WTD) Wear track width (WTW) Worn area (Area) Surface roughness (Ra): ISO 4287 standard	

reduces friction pair wear rate and extends service life [11–15]. Marian et al. [16] reviewed the beneficial properties of layered 2D materials that enable the control of their tribological behavior and make them excellent candidates for effective friction and wear enhancement in dry-running and boundary lubricated machine components. This study proves great potential for 2D materials in this field. Furthermore, 2D materials exhibit advantageous thermal and electrical properties, even under extreme conditions [11]. Moreover, the majority of 2D materials exhibit remarkable resilience to elevated temperatures, high contact pressures, and electrical discharges [11]. These attributes ensure prolonged lubricity, thereby preserving their functionality even in scenarios where base lubricants become ineffective due to these extreme conditions.

MXenes ($M_{n+1}X_nT_x$, being M a transition metal, X is C and/or N, and T a surface end), are one of the newfound and fastest developing of 2D-materials class. These environmentally friendly materials own graphene-like form with analogous mechanical assets, ample surface terminations T (for example -O, -OH, -F), little shear strength as well as exceptional lubrication capability [17]. MXenes are contemplated as potential applicants for use as lubricant additives. These 2D nanomaterials can adhere to metallic surfaces to passivate the contact, thereby reducing the interface adhesion and enhancing friction and wear properties [18]. Although their investigation is still scarce, some recent studies demonstrate that MXenes and their derivatives can successfully enhance the tribological performance of different lubricants [19–22], being necessary further investigations. Thus, Liu et al. [21] analyzed friction and wear performance, with a friction pair of 32100 bearing steel, of a polyalphaolefin (PAO8) additivated with $Ti_3C_2T_x$ nanosheets, resulting in friction and wear decreases around 10 % for the

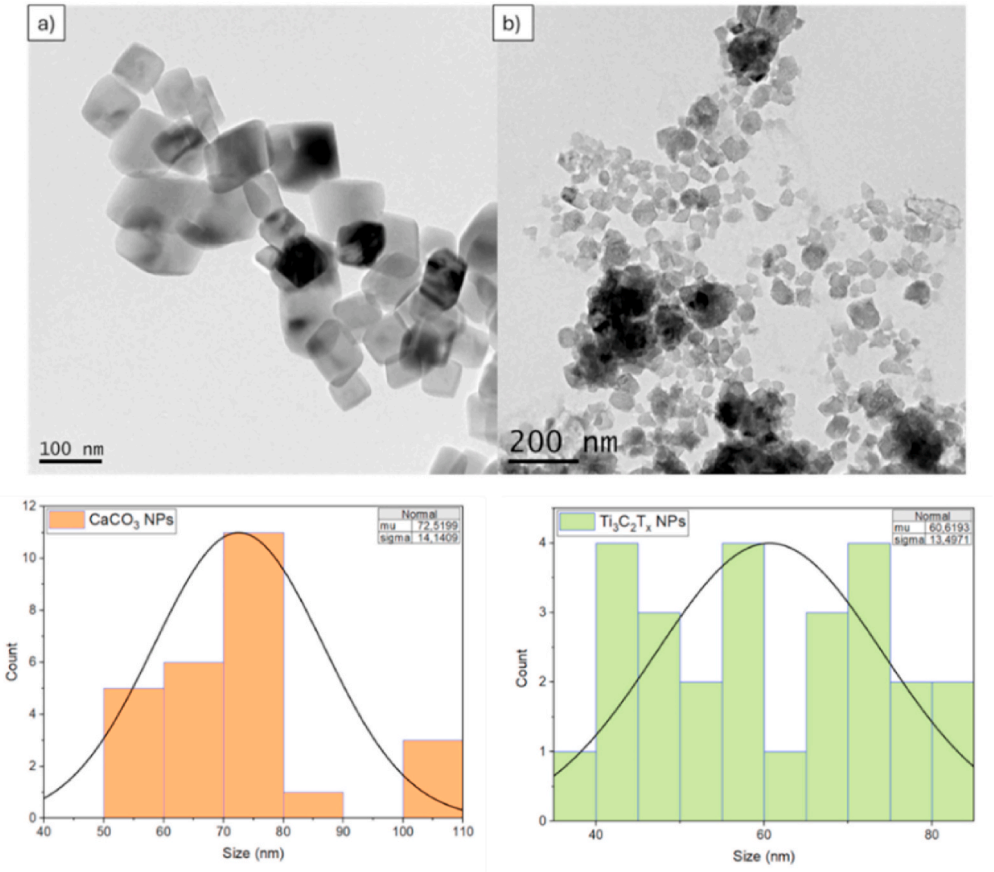

Fig. 3. TEM micrographs and distribution of synthesized $CaCO_3$-OA (a) and $Ti_3C_2T_x$ (b) NPs.

optimal nanolubricant (0.8 wt%). Furthermore, Boidi et al. [23] studied the Stribeck curves of two nanodispersions of $Ti_3C_2T_x$ nanosheets (0.5 wt % and 3.0 wt%) in PAO8 varying speed, load (5, 10 and 28 N), SRR (from 0 to 100 %), and temperature conditions (25, 40 and 100 °C) of the friction test conducted on a AISI 52100 steel tribopair. These authors found that for the two higher temperatures and loads, the friction coefficients observed in the range 0–10 % SRR with both nanodispersions were higher than those corresponding to PAO8, improving the results at 100 °C when the SRR increases. Wa et al. [24] studied the tribological performance of the system $Ti_3C_2T_x$ nanosheets with N, N-dimethylformamide as a dispersion aid in a 5750 oil. These authors found that MXenes based nanolubricants have better wear reduction and antiwear performance compared to 5750 oil, with a reduced wear rate of 92 %, proving that MXenes have great advantages and potential as a lubricating additive. Furthermore, Cui et al. [25] investigated the tribological performance of MXene and phenolic resin modified polytetrafluoroethylene composites, MXene@mPTFE, as additives of a low viscosity PAO (PAO6). These authors found excellent tribological performance, with the coefficient of friction decreased from 0.644 to 0.111, the wear volume decreased by 93 %, and the bearing capacity increased to 750 N. Finally, Gao et al. [26] studied the tribological performance of functionalized MXenes with dialkyl dithiophosphate (DDP-$Ti_3C_2T_x$) finding significant antiwear and friction reduction abilities, with a low coefficient of friction not exceeding 0.11 and a decrease in the wear volume by 87 %. These excellent tribological properties may be attributable to the good dispersion and the shape of the small sheets, which ensure the formation of a continuous chemical protective film that prevents direct contact and seizure.

Another promising environmentally friendly nanomaterial is calcium carbonate NPs, $CaCO_3$, which has a low toxicological profile and thus meets European Ecolabel standards for utilize as additives in lubricant [27]. These NPs are commonly utilized in the automotive industry, adhesives, inks, and as lubricant additives. However, despite the limited number of tribological studies on $CaCO_3$ NPs as lubricant additives, some authors found noteworthy tribological results using these NPs as oil additives. For instance, Zhang et al. [28] reported a 90 % reduction in wear volume when 1 wt% $CaCO_3$ NPs have been utilized as additives of a PAO10 oil. Furthermore, Sunqing et al. [29] explored the tribological properties of 500SN oil and $CaCO_3$ NPs as additives, reaching remarkable friction and wear reductions when mass concentrations were between 0.2 and 1 wt%. Finally, Kulkarni et al. [30] analyzed the tribological properties of $CaCO_3$ NPs as jojoba oil additives, finding decreases in friction and wear about 35 % and 40 %, correspondingly. Nevertheless, in literature there is just one investigation that utilizes functionalized $CaCO_3$ NPs as lubricant additives [31].

Given the scarcity of experimental works on tribological behavior of MXenes and $CaCO_3$ NPs as lubricant additives, it is necessary to conduct further research on these lubricant additives to develop potential low-viscosity transmission fluids for electric vehicles. Therefore, here the tribological characterization of PAO8 base oil (low viscosity) containing two different nanomaterials: $Ti_3C_2T_x$ (layer nanosheets), functionalized $CaCO_3$ (nanoparticles) or their mixture (hybrid additives) was performed to study the potential of these nanopowders as lubricant additives and the possible tribological synergies between $CaCO_3$ and $Ti_3C_2T_x$ nanomaterials, giving originality to this work.

2. Material and experimental techniques

2.1. PAO8 oil and synthetized NPs

PAO8 base oil, provided by REPSOL, with viscosity index of 138 as well as a viscosity and density of 39.47 mPa s and 0.8163 g cm^{-3},

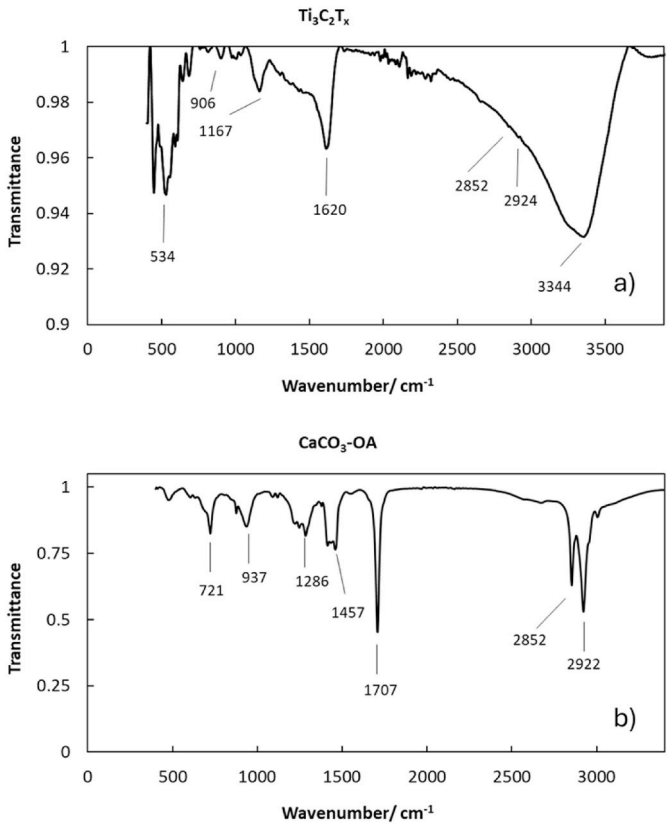

Fig. 4. FTIR characterization of synthesized MXene $Ti_3C_2T_x$ (a) and $CaCO_3$-OA (b) NPs.

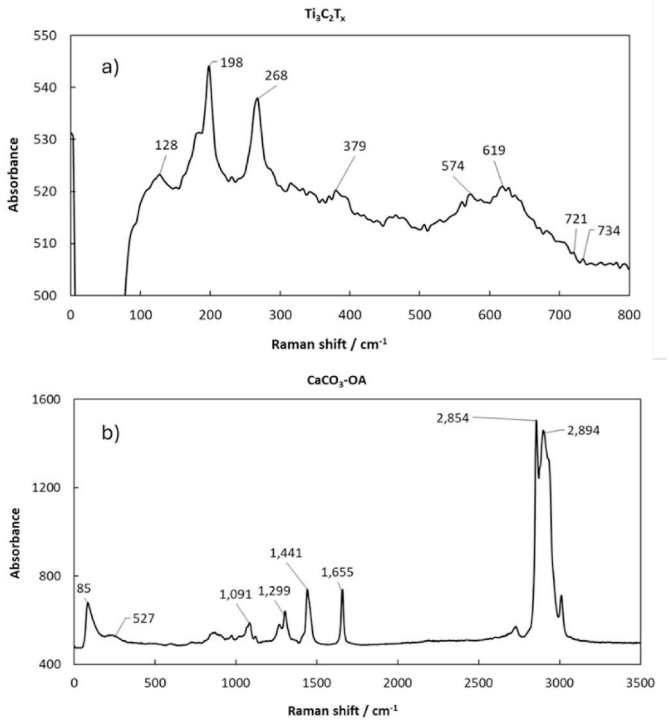

Fig. 5. Raman characterization for synthesized MXene $Ti_3C_2T_x$ (a) and $CaCO_3$-OA (b) NPs.

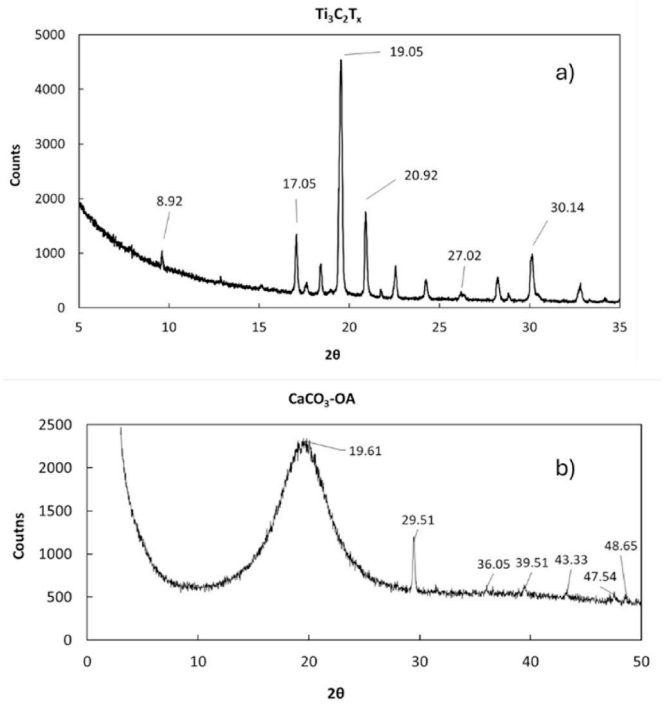

Fig. 6. XRD patterns of synthesized MXene (a) and $CaCO_3$-OA (b) nanomaterials.

correspondingly, at 313.15 K [32], was utilized. With regard to the used nanoadditives, both $CaCO_3$-OA and $Ti_3C_2T_x$ NPs were synthesized and fully characterized.

The synthesis of the $CaCO_3$-OA NPs was conducted in accordance with the procedure depicted in Fig. 1. Firstly, $Ca(NO_3)_2$ was synthesized using NaOH 0.2M, Na_2CO_3 0.1 M and $NaNO_3$ 0.2M solutions. Thus, Na_2CO_3 0.1 M was dispersed in deionized water with NaOH and $NaNO_3$, being the NaOH added to achieve alkaline pH suitable for Na_2CO_3 precipitation and the $NaNO_3$ to decrease the solubility of $Ca(NO_3)_2$ by the common ion effect [33]. Subsequently, a $Ca(NO_3)_2$ 0.2 M solution was added dropwise to Na_2CO_3 solution, and it was maintained under continuous stirring (750 rpm) at room temperature around 120 min. Finally, the resultant mixture was poured into a separatory funnel, permitting the $CaCO_3$ NPs to precipitate, and dried at room temperature. Once these $CaCO_3$ NPs were obtained, their functionalization was carried out in accordance with a similar procedure to that described by Wang et al. [34]. For this task, 3 mL of oleic acid (OA) modifier were dispersed in $CHCl_3$, and the mixture was inserted in a flask. Afterwards, 1 g of previously obtained $CaCO_3$ NPs was also added and mixed for 1 h under agitation, maintaining it at room temperature throughout the whole process. Finally, the $CHCl_3$ was evaporated through a rotary evaporator, resulting in the desired $CaCO_3$-OA NPs.

The synthesis of $Ti_3C_2T_x$ MXene nanosheets (Fig. 2) was carried out with a method comparable to that proposed by Zaharin et al. [35]. Briefly, this synthesis begins with the preparation of two aqueous solutions of LiF 2.5 M and HCl 6 M. These are combined according with the first reaction indicated in Fig. 2. Subsequently, 1.0 g of commercial Ti_3AlC_2 (from Sigma Aldrich) is included slowly to LiCl/HF solution in order to prevent any adverse risks that might arise of the exothermic reaction. This mixture was maintained under magnetic stirring during 30 min followed by other 30 min of ultrasonic agitation. Then, the mixture was introduced in the microwave oven to perform the chemical reaction at 30 °C for 10 min. Lastly, the acidic blend was washed with deionized water and ethanol various times till reaching a pH > 5.0. After that, the MXene solution was centrifuged for 5 min at 5000 rpm to finally carry out a lyophilization process with the aim of obtaining the

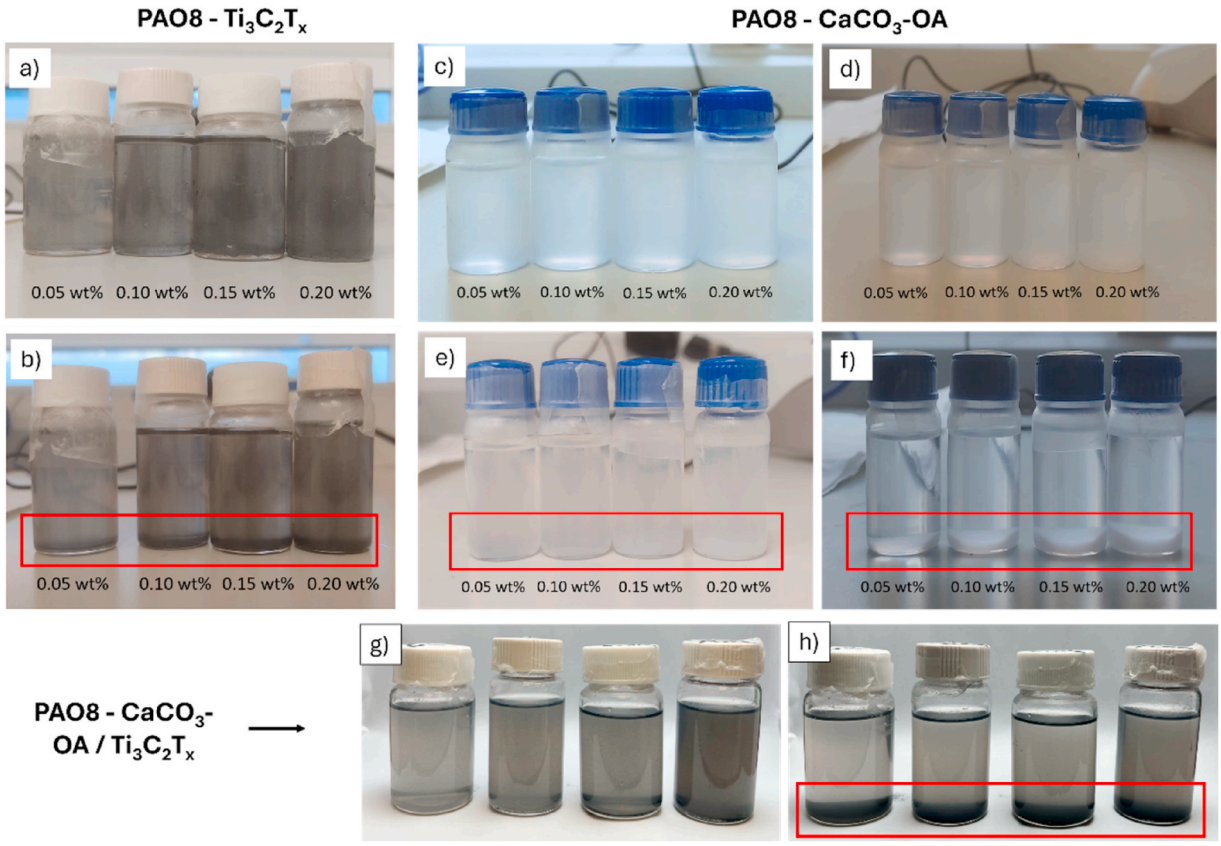

Fig. 7. Visual stability of $Ti_3C_2T_x$ nanolubricants after 0 h (a) and 24 h (b), $CaCO_3$-OA nanolubricants after 0 h (c), 24 h (d), 48 h (e) and 72 h (f) and hybrid lubricants after 0 h (g) and 24 h (h).

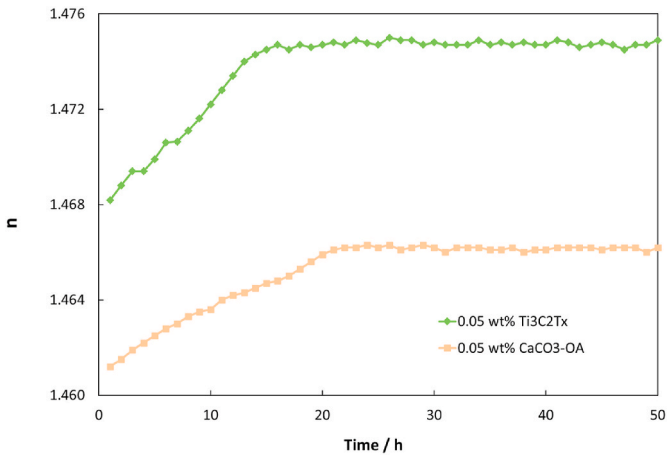

Fig. 8. Refractive index evolution for $Ti_3C_2T_x$ and $CaCO_3$-OA nanolubricants.

$Ti_3C_2T_x$ MXene NPs as a black powder.

2.2. Preparation of nanolubricants

Nanodispersions based on $Ti_3C_2T_x$ nanosheets, $CaCO_3$-OA and hybrid $CaCO_3$-OA/$Ti_3C_2T_x$ NPs were formulated using the following mass concentrations: 0.05 %, 0.10 %, 0.15 % and 0.20 % in PAO8 base, to discover the optimal concentration with the greatest friction and wear properties. In case of hybrid additives, the same mass was added for both NPs. To prepare the potential nanolubricants the conventional two-step method was employed, being the NPs ($Ti_3C_2T_x$ or/and $CaCO_3$-OA) added to the PAO8 base oil. In order to achieve homogeneity of the nanolubricants, ultrasonic treatment is required which was performed by means of a Fisherbrand FB11203 ultrasonic bath for a period of 3 h and changing the water to avoid the overheating of lubricant samples. Following the preparation of the nanolubricants, an investigation was conducted into their temporal stability, employing visual control and refractometry.

2.3. Tribological characterization

Friction experiments with PAO8 and $Ti_3C_2T_x$ and $CaCO_3$-OA nanolubricants were done with a tribology cell T-PTD200 connected with an Anton Paar MCR 302 rheometer operating in a ball-on-three-pins rotational design. Further details regarding friction measurements can be located in Table 1 and in previous research paper [36]. Three replicates were done for each lubricant sample to reach representative values of the average friction coefficient. Lastly, the wear caused in pins and balls during these experiments was characterized by a 3D optical profilometer using various parameters, which are outlined in Table 1 together with the measurement conditions. Furthermore, a confocal Raman microscope (WITec alpha300R+) and SEM microscope were employed to inspect the worn surfaces and achieve information about the tribological mechanisms that could occur.

3. Results and discussion

3.1. Characterization of synthesized NPs

The synthesized nanomaterials ($CaCO_3$-OA and $Ti_3C_2T_x$ nanosheets) were characterized by means of diverse techniques, like transmission electron microscopy (TEM) to know their appearance and dimensions, Raman and infrared spectroscopy (FTIR) to identify the principal functional groups and X-ray powder diffraction (XRD) to obtain information

Table 2
Mean friction coefficients, μ, wear scar diameter, WSD, wear track depth, WTD and worn transversal areas of pins together with their standard deviations, σ, for $Ti_3C_2T_x$ and $CaCO_3$-OA nanolubricants.

	μ	σ	WSD/μm	σ/μm	WTD/μm	σ/μm	Area/μm^2	σ/μm^2
PAO8	0.137	0.009	572	22	4.08	0.03	1547	37
+0.05 wt% $Ti_3C_2T_x$	0.144	0.002	528	22	4.08	0.23	1434	83
+0.10 wt% $Ti_3C_2T_x$	0.143	0.002	490	21	4.00	0.20	1293	91
+0.15 wt% $Ti_3C_2T_x$	0.143	0.002	617	10	6.94	0.41	2923	246
+0.20 wt% $Ti_3C_2T_x$	0.161	0.003	595	28	4.56	0.40	1756	214
+0.05 wt% $CaCO_3$-OA	0.083	0.003	572	48	5.50	0.99	2156	551
+0.10 wt% $CaCO_3$-OA	0.076	0.002	540	11	4.68	0.23	1700	121
+0.15 wt% $CaCO_3$-OA	0.090	0.004	420	28	2.18	0.34	601	127
+0.20 wt% $CaCO_3$-OA	0.095	0.009	420	33	2.16	0.26	606	118
+0.05 wt% $CaCO_3$-OA/$Ti_3C_2T_x$	0.147	0.002	525	16	4.50	0.99	1553	412
+0.10 wt% $CaCO_3$-OA/$Ti_3C_2T_x$	0.140	0.001	498	22	3.68	0.23	1242	124
+0.15 wt% $CaCO_3$-OA/$Ti_3C_2T_x$	0.139	0.001	515	15	4.18	0.34	1201	115
+0.20 wt% $CaCO_3$-OA/$Ti_3C_2T_x$	0.141	0.001	530	20	4.16	0.26	1304	108

of their crystallinity. Fig. 3 displays the appearance of $CaCO_3$-OA and $Ti_3C_2T_x$ NPs through TEM images and their respective size distributions, which were obtained through the Image J software. Thus, the $CaCO_3$-OA NPs show a perfect cubic shape and average size around 70 nm, whereas the $Ti_3C_2T_x$ nanosheets have a laminar flake-like structure with sizes mainly around 40–75 nm, similar TEM images of $Ti_3C_2T_x$ MXenes were recently found by Kamal Kamarulzaman et al. [17].

Furthermore, to find information regarding functional groups of NPs, FTIR spectroscopy was used. Thus, Fig. 4a exhibits the FTIR spectrum of $Ti_3C_2T_x$, in which the absorption bands at 3344 and 1620 cm^{-1} are given to the stretching -OH, which has strong hydrogen bonds, and bending of C-OH group, correspondingly. In addition, the bands located at 2924 and 2852 cm^{-1} are recognized to C-H bond stretching (symmetric and asymmetric), while the peak at 1167 cm^{-1} is given by C-F bond stretching. In addition, the deformation of Ti-O-Ti bond and Ti-O bond may be responsible for the peaks at 906 and 534 cm^{-1}, respectively. All the peaks that appear in the FTIR spectrum show good correspondence with previous characterizations of $Ti_3C_2T_x$ [37]. Hence, it is likely that the surface of $Ti_3C_2T_x$ contains -F, -H, -O elements or -OH groups. With regard to the FTIR spectrum of $CaCO_3$-OA NPs, Fig. 4b exhibits an intense peak at 1707 cm^{-1} that matches with the deprotonated carboxyl group (typical position around 1710 cm^{-1}). If this functional group was protonated, a broad and intense band between 2500 and 3500 cm^{-1} would have been observed. Thus, it is confirmed the coating of oleic acid is bound to the calcium carbonate particles through an ionic interaction between the -COO- group of oleic acid and the Ca^{2+} cation. Furthermore, the intense peaks around 2850 and 2922 cm^{-1} are attributed to C-H bonds of an alkyl chain that further confirms the presence of oleic acid on the calcium carbonate surface. The peaks and bands observed in the region below 1500 cm^{-1} are located within the so-called fingerprint zone. The carbonate (CO_3^{2-}) peaks at 1457 cm^{-1} (asymmetric C-O stretching), 937 cm^{-1} (out-of-plane vibration) and 721 cm^{-1} (in-plane vibration) are associated with calcite ($CaCO_3$) [38]. These obtained FTIR results show a high correlation with those reported by Shentu et al. [39] for the $CaCO_3$-OA NPs.

Regarding the Raman characterization of $Ti_3C_2T_x$, Fig. 5a shows the Raman spectrum of these nanosheets performed with a 532 nm laser. A particularly pronounced band is observed at 198 cm^{-1} that is related to out of plane vibrations of C and Ti atoms, corroborating the successful synthesis of $Ti_3C_2T_x$ nanosheets [40]. Furthermore, other bands at 128, 268, 379, 574, 619, 721 and 734 cm^{-1} are also observed. The signals in section 220–480 cm^{-1} correspond to in-plane vibrations (E_g) of surface groups linked to Ti, whereas those of the area among 570 and 740 cm^{-1} are ascribed generally to E_g and A_{1g} carbon vibrations. Thus, these results have a high correspondence with those previously obtained by other researchers for other $Ti_3C_2T_x$ nanosheets [40,41]. Regarding the Raman analysis of $CaCO_3$-OA (Fig. 5b), the spectrum displays very intense peaks at 2854 and 2894 cm^{-1} that are associated to $\nu_s(CH_2)$ and ν(=C–H), respectively [42]. In addition, 1655 cm^{-1} band is attributed to ν(C=O), which corroborates the successful functionalization of $CaCO_3$ NPs with OA [42]. Additionally, peaks related to $CaCO_3$ appear at 285, 715, and 1091 cm^{-1} [43].

Additionally the synthesized nanomaterials were characterized through X-ray diffraction, and the resulting XRD spectrum of the $Ti_3C_2T_x$ and $CaCO_3$-OA nanomaterials are presented in Fig. 6a and b, respectively. This analysis was done with a Bruker D8 Advance. XRD pattern of $Ti_3C_2T_x$ MXene nanosheets exhibits peaks at 2θ = 8.9°, 17.0° 19.0°, 20.9° and 30.1°. Thus, owing to Ti_3C_2Al starting substance reacting with HF, peaks were substantially changed to inferior angles (8.9° and 19.0°) in XRD pattern of $Ti_3C_2T_x$. This change indicates an expanded spacing in MXene compared to the starting Ti_3AlC_2 compound [40]. Additionally, a new peak at 27.0° (008) has been detected; which can be attributed to $Ti_3C_2(OH)_2$ creation, in accordance with findings described by Li et al. [44]. Moreover, the presence of extra peaks was ascribed to residual Al in the $Ti_3C_2T_x$ that is difficult to remove entirely and forms AlF_3 [45,46]. Concerning XRD pattern of $CaCO_3$-OA NPs, Fig. 5b, peaks were observed at 2θ = 19.6°, 29.5°, 36.1°, 39.5°, 43.3°, 47.5°, and 48.7°, which correspond to the (012), (104), (110), (113), (202), (018) and (016) crystal planes [47]. Therefore, the XRD spectrum matches with 98–004-0107 ICSD Card of Calcite [47]. Due to functionalization of $CaCO_3$-OA NPs, intensity of XRD peaks is considerably reduced in comparison with bare $CaCO_3$ [48].

3.2. Nanolubricants stability

Fig. 7 illustrates the visual stability control of the nanodispersions, observing that for $CaCO_3$-OA nanolubricants, the stability is better compared to $Ti_3C_2T_x$ and hybrid $CaCO_3$-OA/$Ti_3C_2T_x$ nanolubricants. Thus, Fig. 7b and h shows that the $Ti_3C_2T_x$ nanosheets and hybrid $CaCO_3$-OA/$Ti_3C_2T_x$ nanoadditives seem to be sedimented after 24 h whereas in the case of $CaCO_3$-OA NPs the sedimentation starts to appear after 48 h (Fig. 7e).

With the aim of quantifying the stability of $CaCO_3$-OA and $Ti_3C_2T_x$ nanolubricants refractometry technique was employed. Therefore, Fig. 8 depicts the progression of the refractive index for the 0.05 wt% $CaCO_3$-OA and $Ti_3C_2T_x$ nanolubricants. For 0.05 wt% $Ti_3C_2T_x$ nanodispersion after the first 10 h the $Ti_3C_2T_x$ nanosheets seem to be fully sedimented, while for the 0.05 wt% $CaCO_3$-OA nanodispersion the sedimentation rate is slower. Precisely, for the $Ti_3C_2T_x$ nanolubricant the refractive index raised 0.30 % after 10 h of study whereas for $CaCO_3$-OA nanolubricant it raised only 0.16 %. This fact evidenced that the oleic acid surface modification certainly improves the stability of nanolubricants.

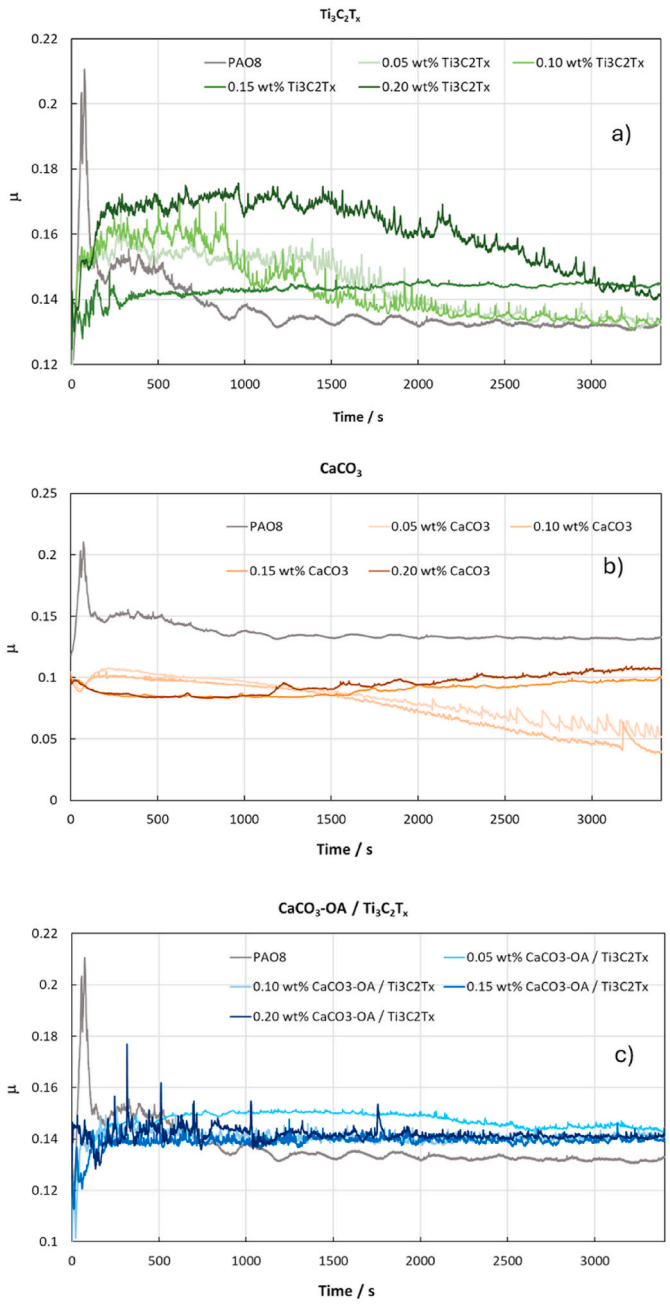

Fig. 9. Friction coefficients, μ, achieved over time for PAO8 base oil and $Ti_3C_2T_x$ (a) $CaCO_3$-OA (b) and hybrid $CaCO_3$-OA/$Ti_3C_2T_x$ (c) nanolubricants.

3.3. Friction and wear properties of nanolubricants

Friction analyses were performed with PAO8 base oil, $Ti_3C_2T_x$ nanolubricants, $CaCO_3$-OA nanolubricants, and hybrid $Ti_3C_2T_x$/$CaCO_3$-OA nanolubricants with mass concentrations of 0.05 wt %, 0.10 wt %, 0.15 wt% and 0.20 wt% using the tribometer previously described. For the hybrid additives the same mass was added for both NPs. The average values of the friction coefficient, μ, are reported for all lubricant samples in Table 2. As illustrated in Figs. 9 and 10, nanolubricants containing $Ti_3C_2T_x$ nanosheets or hybrid nanoadditives did not reduce the coefficient of friction compared to PAO8 oil. In contrast, the incorporation of $CaCO_3$-OA NPs led to a notable enhancement in friction, with a maximum friction decrease of 44 % for the greatest concentration of 0.10 wt% $CaCO_3$-OA. Thus, Figs. 9 and 10 also demonstrate advanced antifriction performance for $CaCO_3$-OA nanolubricants in comparison to

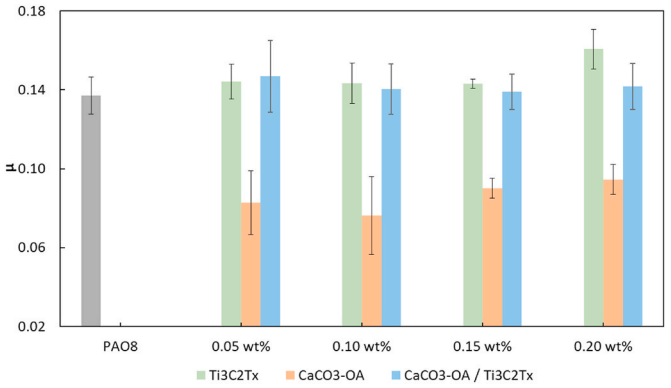

Fig. 10. Average friction coefficients, μ, obtained with the base oil and its nanolubricants.

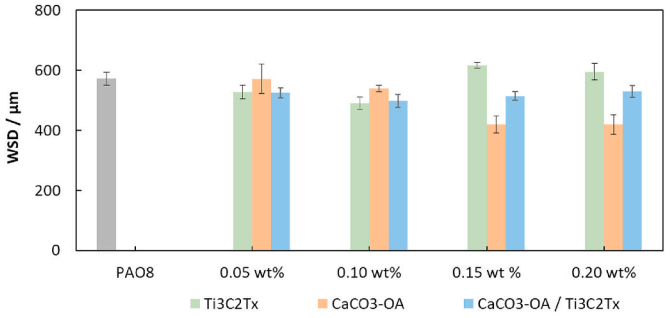

Fig. 11. Average WSD observed in pins lubricated with PAO8 and its $Ti_3C_2T_x$ and $CaCO_3$-OA nanolubricants.

those containing $Ti_3C_2T_x$ nanosheets or hybrid nanoadditives. Moreover, $CaCO_3$-OA NPs decreases the friction for all the mass concentrations. However, beyond the best concentration (0.10 wt%), friction reductions worsen a bit (from 44 % for the optimal to 31 % for the highest mass concentration). Regarding the $Ti_3C_2T_x$ nanolubricants, a similar trend was observed, obtaining the worst antifriction performance with the highest mass concentration. These results may be explained as an excess of NPs beyond the greatest concentration could origin little agglomeration that provokes a drop in the tribological behavior of $CaCO_3$-OA and $Ti_3C_2T_x$ nanolubricants, as evidenced in certain studies [49,50]. For hybrid nanolubricants, similar friction values were found for all mass concentrations and base oil (Fig. 9c), demonstrating that there are no antifriction synergies between $CaCO_3$-OA and $Ti_3C_2T_x$ nanoadditives.

As can be observed in Table 2 and Fig. 11, the use of $Ti_3C_2T_x$ and $CaCO_3$-OA nanomaterials with PAO8 leads to a substantial improvement in antiwear behavior compared to the base oil without nanoadditives. Particularly, the biggest wear decreases were reached for $CaCO_3$-OA nanolubricants, with maximum wear reductions at a mass concentration of 0.15 wt%: 27 % in terms of WSD, 47 % in WTD, and 61 % in the worn area. The best antiwear performance for these $CaCO_3$-OA nanolubricants was achieved at high concentrations (0.15 wt% and 0.20 wt%). At small $CaCO_3$-OA concentrations (0.05 and 0.10 wt%), NPs can certainly be dispersed in PAO8 oil, nevertheless NPs do not protect entirely metal surfaces; consequently, the uncovered surfaces would slide between them producing wear. Therefore, only a minor decrease in wear is detected (6 %). When $CaCO_3$-OA NPs concentration rises (0.15 wt%), the wear improvement is significant. This circumstance could be due to the filling of $CaCO_3$-OA NPs on metal surfaces up to a saturation point is reached. At highest concentration (0.20 wt%), the excess of NPs can provoke a bit drop in the wear improvement, since they may operate in a similar manner to debris particles, creating abrasive wear. The greatest

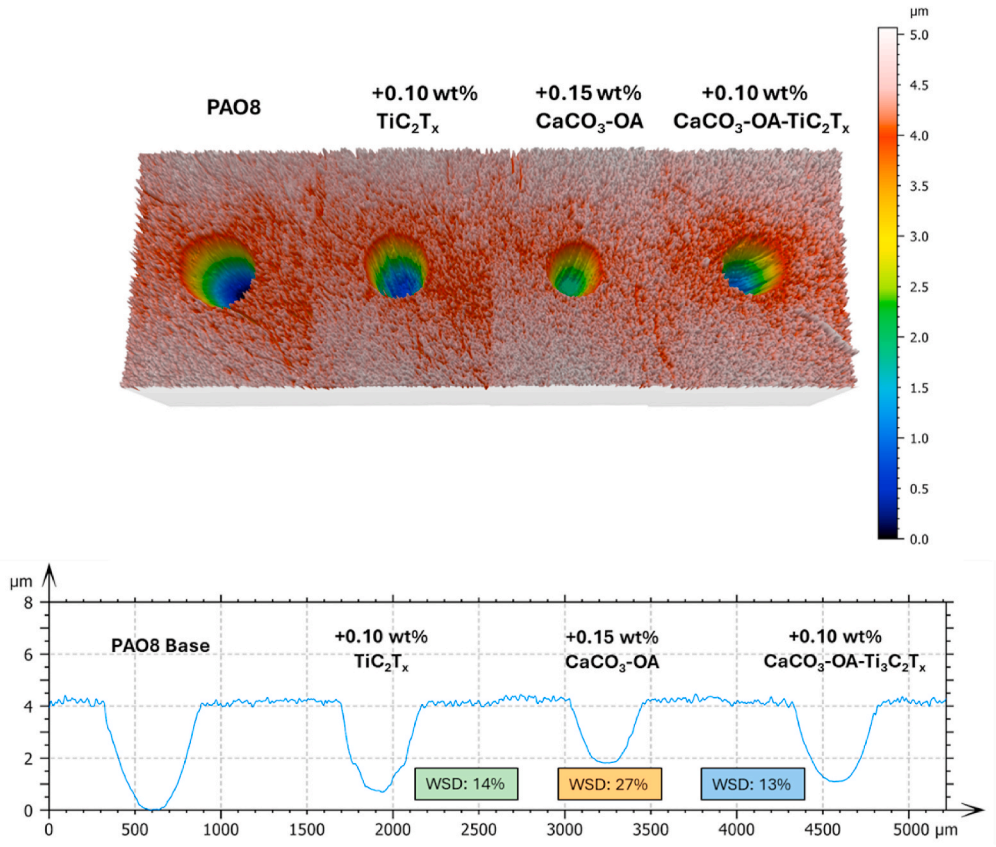

Fig. 12. 3D mapping and 2D section profile of surfaces of the pins tested with the optimal $Ti_3C_2T_x$ and $CaCO_3$-OA nanolubricants and PAO8.

Table 3
Wear track width, WTW and wear track depth, WTD, of balls together with their standard deviations, σ, tested with $Ti_3C_2T_x$, $CaCO_3$-OA and hybrid nanolubricants.

	WTW/μm	σ/μm	WTD/μm	σ/μm
PAO8	462	36	150	21
+0.05 wt% $Ti_3C_2T_x$	428	23	122	15
+0.10 wt% $Ti_3C_2T_x$	448	27	125	16
+0.15 wt% $Ti_3C_2T_x$	513	15	113	18
+0.20 wt% $Ti_3C_2T_x$	495	27	145	18
+0.05 wt% $CaCO_3$-OA	272	24	68	9
+0.10 wt% $CaCO_3$-OA	245	11	62	10
+0.15 wt% $CaCO_3$-OA	184	12	53	7
+0.20 wt% $CaCO_3$-OA	265	26	61	8
+0.05 wt% $CaCO_3$ -OA/$Ti_3C_2T_x$	449	21	64	11
+0.10 wt% $CaCO_3$-OA/$Ti_3C_2T_x$	446	21	67	5
+0.15 wt% $CaCO_3$-OA/$Ti_3C_2T_x$	482	12	78	9
+0.20 wt% $CaCO_3$-OA/$Ti_3C_2T_x$	467	35	72	8

antiwear performance for a medium mass concentration has also been noted in other investigations [49,50]. Regarding the $Ti_3C_2T_x$ nanolubricants, wear improvements were achieved at low concentrations (0.05 and 0.10 wt%) with the greatest behavior for the 0.10 wt% nanolubricant: 14 % in terms of WSD, 2 % in WTD, and 16 % in the worn area. Finally, for hybrid nanolubricants, slight wear improvements were found for all the mass concentrations with the greatest behavior for the 0.10 wt% nanolubricant: 13 % in terms of WSD, 10 % in WTD, and 20 % in the worn area. Therefore, the hybrid nanolubricants have better the antiwear performance than the PAO8 base oil and $Ti_3C_2T_x$ nanolubricants, but worse than the $CaCO_3$-OA nanolubricants.

To better distinguish the wear enhancements, Fig. 12 displays the worn surface profiles achieved with the pins lubricated with PAO8, the best nanolubricants of $Ti_3C_2T_x$ (0.10 wt%), of $CaCO_3$-OA (0.15 wt%) and of the hybrid nanoadditive (0.10 wt%). It is evident that the greatest reductions were achieved with the $CaCO_3$-OA nanolubricants.

Additionally, to better visualize the wear produced by using the different studied lubricants during friction experiments, the upper specimens (balls), lubricated with PAO8 base oil and with the $Ti_3C_2T_x$, $CaCO_3$-OA and hybrid nanolubricants were also analyzed with the profilometer. As Table 3 and Fig. 13 shows, for the ball lubricated with 0.10 wt% $Ti_3C_2T_x$ nanolubricant a slight width wear decrease was observed (3 %), whereas for the ball lubricated with 0.15 wt% $CaCO_3$-OA a great wear decrease was reached (60 %), while for the balls lubricated with hybrid nanolubricants a maximum reduction of 4 % of wear track width was reached (0.10 wt%). These wear results of balls are aligned with the previous ones obtained for worn pins, confirming the better lubrication performance for $CaCO_3$-OA nanolubricants.

Once the friction and wear have been analyzed, it seems clear that $CaCO_3$-OA nanoparticles have better tribological properties than $Ti_3C_2T_x$ nanosheets (both friction and wear). To find out if this better tribological behavior is due to the presence of functionalization, the tribological results of the Mxenes are compared below with those obtained by $CaCO_3$ nanolubricants in PAO8 carried out in a previous study, with the same operating conditions. Thus, Liñeira del Río et al. [51] achieved maximum friction reductions of 13 % for nanolubricants containing 0.05 wt% $CaCO_3$ nanoparticles and greatest wear reductions of 28 % in WSD (0.15 wt % $CaCO_3$). Comparing these previous results with the present work, oleic acid functionalization improves the friction performance (44 % reduction for the optimal concentration of 0.10 wt% $CaCO_3$-OA and 13 % for nanolubricants containing a 0.05 wt% of uncoated $CaCO_3$) but antiwear properties are practically the same (27 % reduction for $CaCO_3$-OA and 28 % for uncoated $CaCO_3$). Based on these results, uncoated $CaCO_3$ NPs have superior lubrication properties than

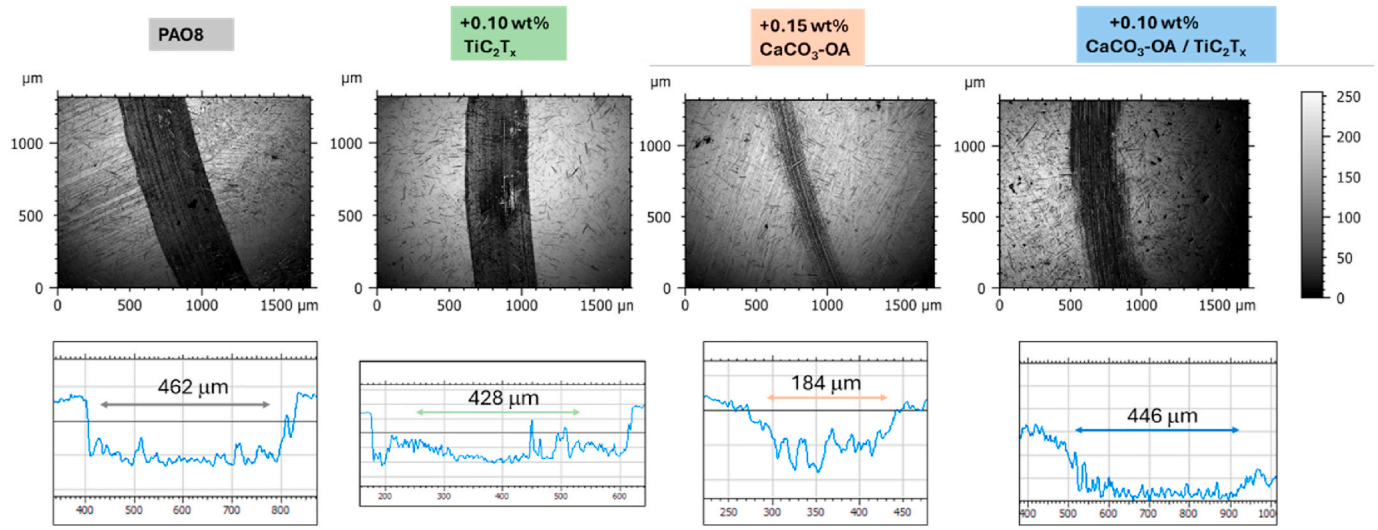

Fig. 13. 2D images of worn balls tested with the $Ti_3C_2T_x$, $CaCO_3$-OA and hybrid nanolubricants with the best antiwear capabilities and with PAO8.

Table 4
Mean roughness, Ra and Rq together with their standard deviations of surfaces lubricated using $Ti_3C_2T_x$, $CaCO_3$-OA, hybrid nanolubricants and PAO8.

	Ra/µm	σ/µm	Rq/µm	σ/µm
PAO8	0.039	0.014	0.048	0.019
+0.05 wt% $Ti_3C_2T_x$	0.031	0.023	0.038	0.029
+0.10 wt% $Ti_3C_2T_x$	0.032	0.010	0.039	0.012
+0.15 wt% $Ti_3C_2T_x$	0.055	0.028	0.066	0.034
+0.20 wt% $Ti_3C_2T_x$	0.069	0.043	0.085	0.052
+0.05 wt% $CaCO_3$-OA	0.031	0.002	0.037	0.002
+0.10 wt% $CaCO_3$-OA	0.032	0.002	0.038	0.002
+0.15 wt% $CaCO_3$-OA	0.013	0.007	0.016	0.008
+0.20 wt% $CaCO_3$-OA	0.014	0.009	0.017	0.012
+0.05 wt% $CaCO_3$ -OA/$Ti_3C_2T_x$	0.035	0.009	0.045	0.011
+0.10 wt% $CaCO_3$-OA/$Ti_3C_2T_x$	0.038	0.012	0.047	0.010
+0.15 wt% $CaCO_3$-OA/$Ti_3C_2T_x$	0.056	0.015	0.068	0.022
+0.20 wt% $CaCO_3$-OA/$Ti_3C_2T_x$	0.064	0.022	0.074	0.021

uncoated $Ti_3C_2T_x$.

3.4. Surface analysis

The study of roughness (Ra and Rq) of worn surfaces was conducted to gain an expanded insight into the antiwear properties of $Ti_3C_2T_x$, $CaCO_3$-OA and hybrid nanolubricants. Three replications were made for PAO8 and each lubricant. As indicated in Table 4, surfaces tested with $CaCO_3$-OA nanolubricants have less roughness than those tested with PAO8. The smoothest surfaces were found for those tested with $CaCO_3$-OA nanolubricants. Precisely, a Ra of 39 nm was reached for the worn track tested with PAO8, while for pin lubricated with optimal 0.15 wt% $CaCO_3$-OA nanolubricant a lowered Ra was achieved (13 nm) that resulted in a 67 % roughness drop. These results demonstrate that $CaCO_3$-OA NPs can act repairing and patching the surfaces obtaining a more regular surface.

With the aim of analyzing the distribution of the $Ti_3C_2T_x$ and $CaCO_3$-OA nanoadditives in the worn surfaces created in friction experiments, Raman mappings of these worn tracks were performed. Firstly, the Raman spectrum of lubricant components, PAO8 [32], $Ti_3C_2T_x$ and $CaCO_3$-OA NPs (Fig. 5) were acquired to recognize them in Raman mappings. These mappings were completed to envisage the surfaces lubricated with nanolubricants exhibiting the greatest tribological operation of $Ti_3C_2T_x$ (0.10 wt%) (Fig. 14a) and of $CaCO_3$-OA (0.15 wt %), (Fig. 14b). Both mappings were conducted by means of a confocal Raman microscope (532 nm). For Raman mapping of surface tested with $Ti_3C_2T_x$ nanolubricant, small green areas that match with the $Ti_3C_2T_x$ spectrum are observed. The $Ti_3C_2T_x$ nanosheets are placed along the furrows of sliding surfaces, demonstrating the formation of a tribofilm, which prevents the metal-metal interaction and reduces the produced wear. The improved tribological properties generated by $Ti_3C_2T_x$ MXene nanoadditives in the base oil are related to the formation of a $Ti_3C_2T_x$-rich tribofilm created by tribochemical reactions. These tribofilms usually contain oxide compounds derived from the counterbody and substrate, which are combined with the structurally degraded MXene nanosheets [18]. Tribofilm growth initiates at the beginning of the friction test, and the greatest behavior is attained when a consistent tribofilm is developed throughout the entire tribological contact. Afterwards, the produced tribofilm is transmitted to the rubbing counterbody, reducing the contact of tribological surfaces, therefore facilitating energy dissipation in tribofilm-tribofilm system. The tribofilms that are produced have easy-to-shear ability, which is a consequence of the weak interflake interactions of the $Ti_3C_2T_x$ MXenes sheets, resulting in a wear reduction [52,53].

Regarding the mapping Raman of the surface tested with $CaCO_3$-OA nanolubricant, Fig. 14b, it can be observed that there are significant green areas placed on the sliding furrows, which correspond to the Raman spectrum of $CaCO_3$-OA NPs. These $CaCO_3$-OA deposits positioned in the sliding path can create a protecting cover of low shear strength within worn surfaces that improves the lubrication properties of PAO8 nanolubricants. Since NPs have high surface energy, they are capable of chemically reacting with the rubbing surfaces to make a tribofilm that minimizes direct contact between surfaces. Considering these facts and the enhanced roughness results (Table 3) for $CaCO_3$-OA nanolubricants, the formation of tribofilm and self-repairing mechanisms are proposed as responsible for the observed improvements. The self-repairing mechanism consists of the nano-sized particles deposited on the contact surface filling the valleys and asperities in the worn surfaces and also compensating for the loss of mass, it is also known as "mending effect" [54]. Similar tribological mechanisms were identified by Sunqing et al. [29] who examined the tribological qualities of $CaCO_3$ NPs as additive of 500SN oil. These authors found that the NPs had decomposed into CaO during friction tests when the temperature and pressure reach a certain level, resulting in the creation of a tribofilm composed by $CaCO_3$ and CaO. Similarly, Zhang et al. [55] examined the antiwear properties of $CaCO_3$ NPs as additives of PAO10 base oil. These authors ascertained that the tribological mechanism is attributable entirely to the deposition of $CaCO_3$ NPs, which results in the film formation of CaO from $CaCO_3$ and other elements on the worn metal

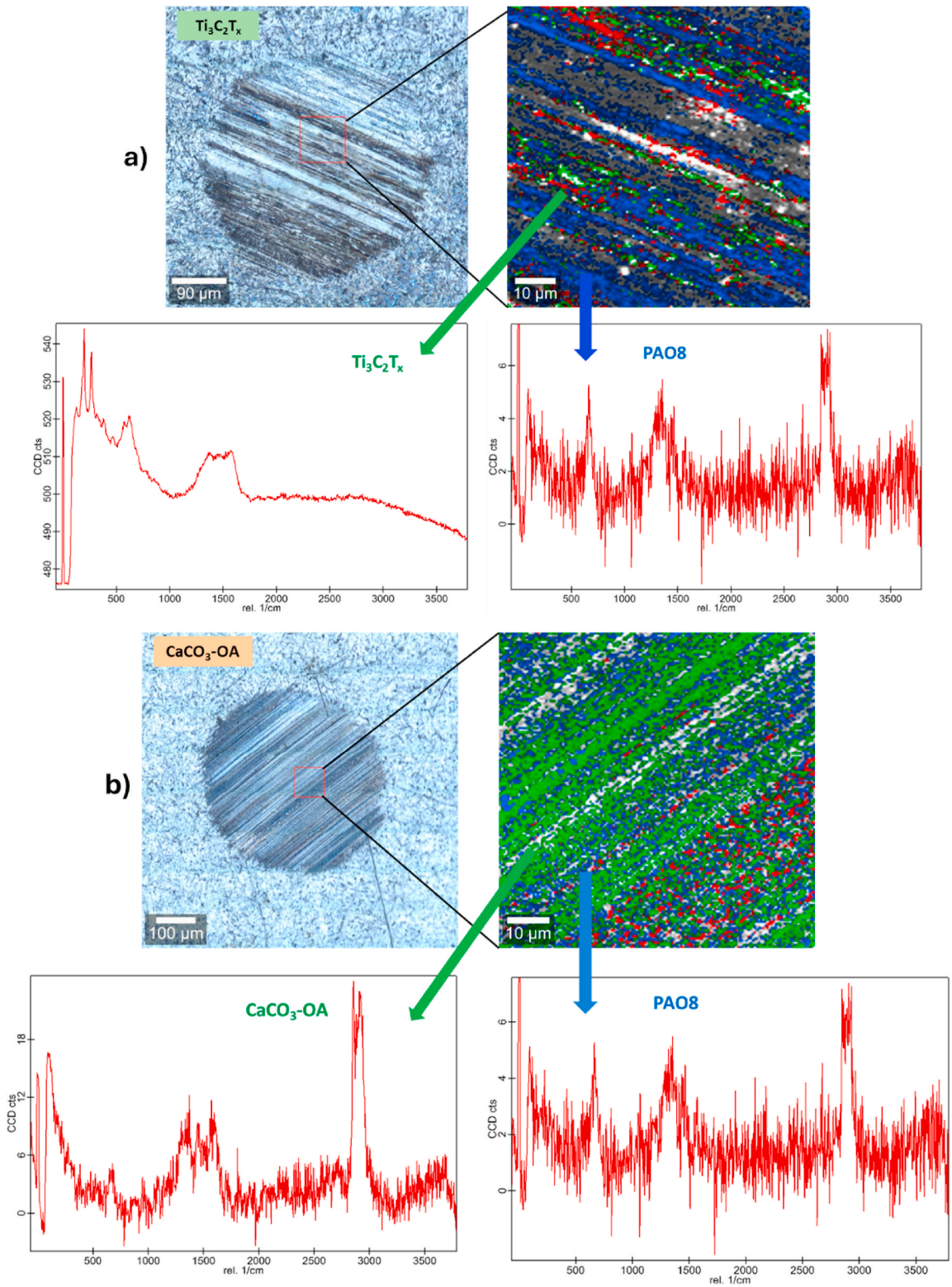

Fig. 14. Raman Mapping of worn pins tested with greatest $Ti_3C_2T_x$ (a) and $CaCO_3$-OA (b) nanolubricants.

surface.

With the aim of expanding the knowledge concerning tribological mechanisms, SEM characterization of pin surfaces tested with PAO8 (Fig. 15a) and optimal nanolubricants PAO8 + 0.10 wt% $Ti_3C_2T_x$ (Fig. 15b) and PAO8 + 0.15 wt% $CaCO_3$-OA NPs (Fig. 15c) was done. As Fig. 15 illustrates, there are grooves in the direction of friction, thus indicating abrasive wear when the PAO8 oil was utilized, as proven by the creation of deep furrows. Nevertheless, in the worn surfaces lubricated with PAO8 containing $Ti_3C_2T_x$ or $CaCO_3$-OA NPs (Fig. 15b and c), the friction surfaces exhibited a notable degree of smoothness, particularly in the case of $CaCO_3$-OA NPs. Regarding $Ti_3C_2T_x$, Ren et al. [56] observed similar behavior for the surfaces of the wear tracks lubricated with $Ti_3C_2T_x$ quantum dots as additives of PEG200 oil. These authors observed that the surfaces became smoother with decreased furrows,

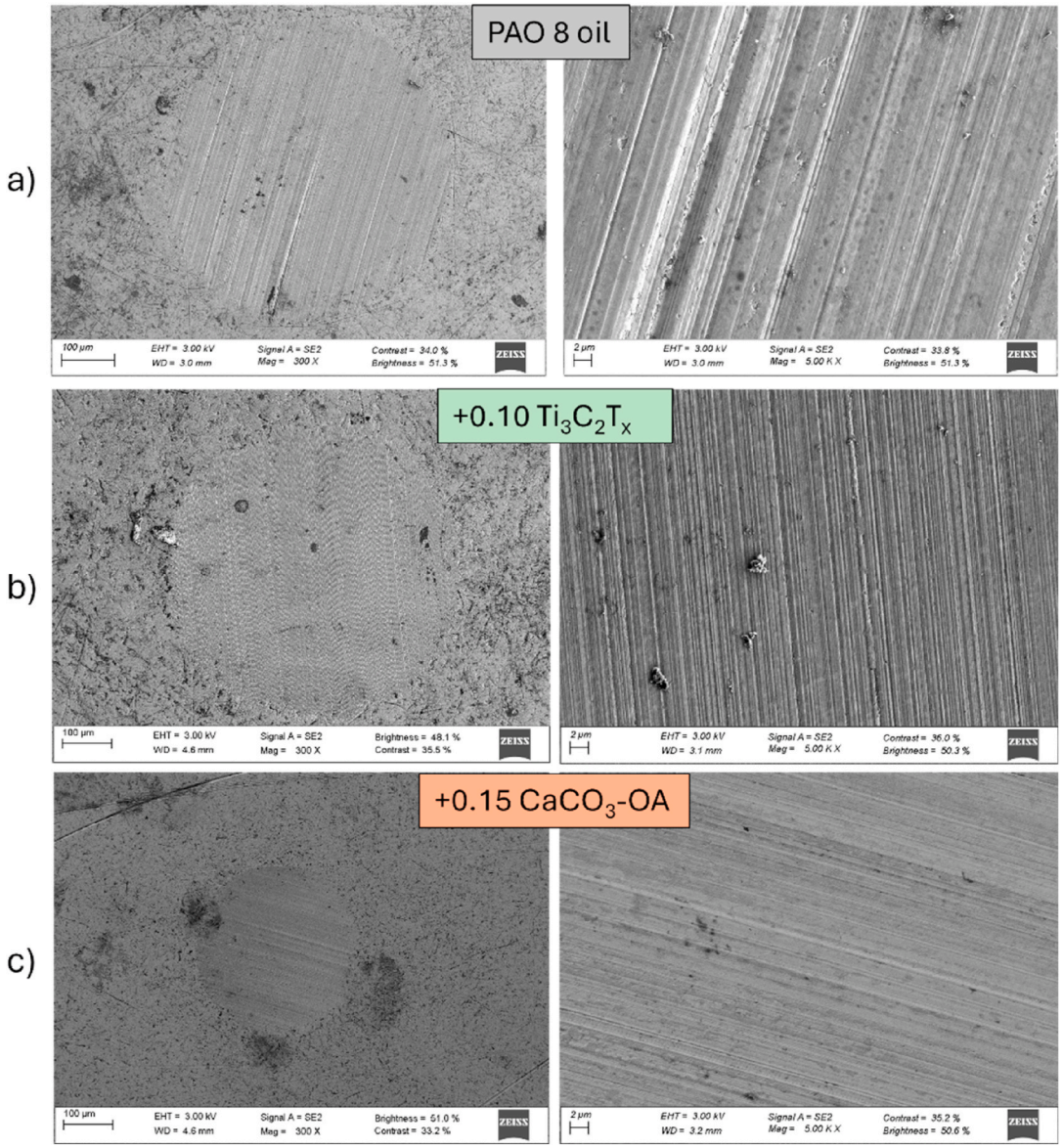

Fig. 15. SEM images of surfaces lubricated by PAO8 base oil (a) and optimal $Ti_3C_2T_x$ (b) and $CaCO_3$-OA (c) nanolubricants.

which were narrower and shallower than those of pure PEG200, being effectively improved. Regarding $CaCO_3$ NPs, similar worn surfaces were observed by Caixiang et al. [57] who observed that the worn surface lubricated with $CaCO_3$ nanolubricants was narrower and flatter than the one obtained with the base oil.

It should be noted that our SEM observations are aligned with the results of the other techniques, which confirm the formation of protective tribofilms containing $Ti_3C_2T_x$ or $CaCO_3$-OA nanoadditives.

In summary, considering the roughness studies, Raman mapping and SEM micrographs of the worn tracks, it was determined that the present tribological mechanisms are tribofilm creation due to the $Ti_3C_2T_x$ nanosheets and tribofilm formation and self-repairing mechanisms for $CaCO_3$-OA NPs. To better visualization, these mechanisms are illustrated in Fig. 16.

4. Conclusions

- $CaCO_3$-OA and $Ti_3C_2T_x$ nanopowders were succesfully synthesized to serve as potential additives for transmission fluids.
- The addition of $CaCO_3$-OA nanoparticles to PAO8 base oil resulted in a notable improvement in friction. The optimal concentration for this enhancement was found to be 0.10 wt% $CaCO_3$-OA, with the greatest decrease of 44 %.
- The addition of $Ti_3C_2T_x$ or $CaCO_3$-OA NPs to PAO8 lead to a considerable enhancement in the antiwear performance compared to base oil, with greatest width wear enhancements of 27 % and 14 % for 0.15 wt% $CaCO_3$-OA and 0.10 wt% $Ti_3C_2T_x$ nanolubricants, respectively.
- Tribological synergies between $CaCO_3$-OA and $Ti_3C_2T_x$ were not found. Hybrid nanolubricants ($CaCO_3$-OA/$Ti_3C_2T_x$) did not present improvements in friction, and they presented slight improvements in wear with the best behavior for the 0.10 wt% nanolubricant (13 % reduction in wear scar diameter).
- Through Raman mapping and roughness evaluation, it was determined that tribological mechanisms which govern the tribological improvement are the tribofilm formation for $Ti_3C_2T_x$ nanolubricants and tribofilm formation and self-repairing for $CaCO_3$-OA nanolubricants.
- $CaCO_3$-OA additives have the potential to remarkably increase the efficiency of transmission fluids of electric vehicles, leading to friction and wear savings and reducing CO_2 emissions.

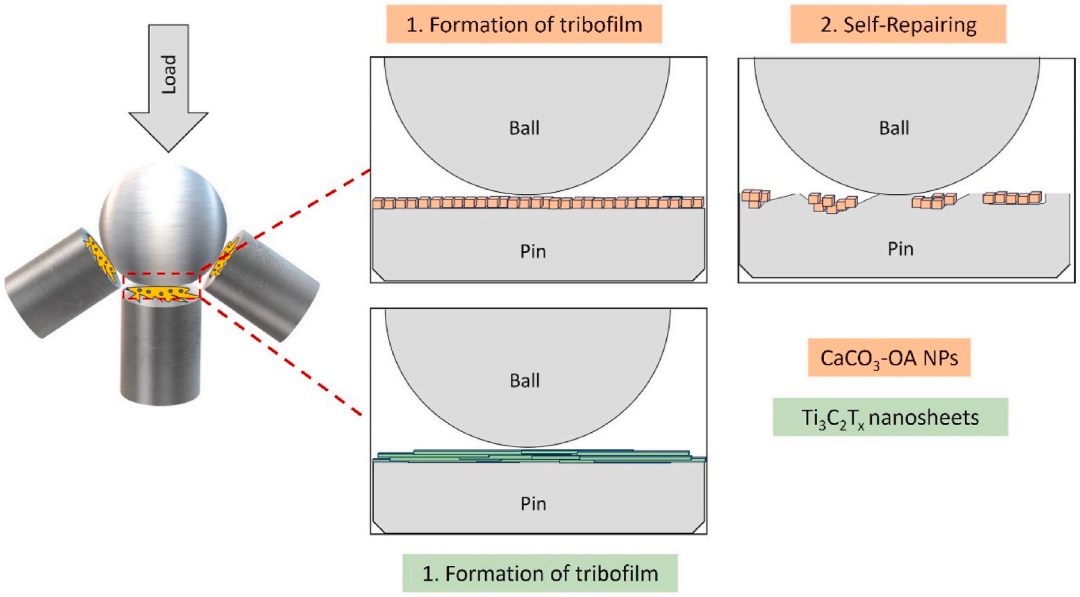

Fig. 16. Scheme of the possible tribological mechanisms for $Ti_3C_2T_x$ and $CaCO_3$-OA NPs in PAO8.

- Prior to the implementation of these nanolubricants in EVs, further research is necessary. This includes tribological tests conducted over extended periods under high loads to assess their potential degradation over time. Additionally, the analysis of the incorporation of supplementary additives, such as viscosity index improvers or corrosion inhibitors, is needed.
- The reduced success of utilizing MXenes as oil additives could be due to their inherent hydrophilicity. However, it is noteworthy that functionalization with non-polar terminations could be a promising avenue for future research.

CRediT authorship contribution statement

José M. Liñeira del Río: Writing – review & editing, Writing – original draft, Supervision, Methodology, Investigation, Formal analysis, Conceptualization. **Martín Gómez Martínez:** Methodology, Investigation, Conceptualization. **Antonio Moreda-Piñeiro:** Writing – review & editing, Supervision. **Enriqueta R. López:** Writing – review & editing, Conceptualization. **Josefa Fernández:** Writing – review & editing, Project administration, Funding acquisition.

Declaration of competing interest

The authors declare that they have no known competing financial interests or personal relationships that could have appeared to influence the work reported in this paper.

Acknowledgments

This research is supported by MCIN/AEI/10.13039/501100011033 through PID2020-112846RB-C22 project and by Xunta de Galicia (ED431C 2024/06). JMLdR is grateful for financial support through the Margarita Salas program, funded by MCIN/AEI/10.13039/501100011033 and "NextGenerationEU/PRTR". Besides, authors are also thankful to Repsol Lubricants for providing the PAO8 base oil and to RIAIDT-USC for its analytical facilities.

Data availability

Data will be made available on request.

References

[1] L.I. Farfan-Cabrera, Tribology of electric vehicles: a review of critical components, current state and future improvement trends, Tribol. Int. 138 (2019) 473–486, https://doi.org/10.1016/j.triboint.2019.06.029.
[2] O.A. Aguilar-Rosas, J.A. Alvis-Sánchez, B. Tormos, B.M. Marín-Santibáñez, J. Pérez-González, L.I. Farfan-Cabrera, Enhancement of low-viscosity synthetic oil using graphene nanoparticles as additives for enduring electrified tribological environments, Tribol. Int. 188 (2023) 108848, https://doi.org/10.1016/j.triboint.2023.108848.
[3] K. Holmberg, A. Erdemir, The impact of tribology on energy use and CO2 emission globally and in combustion engine and electric cars, Tribol. Int. 135 (2019) 389–396, https://doi.org/10.1016/j.triboint.2019.03.024.
[4] A. Gupta, Characterization of engine and transmission lubricants for electric, hybrid, and plug-in hybrid vehicles (Columbus, OH: Ohio State University), Master of Science, 2012.
[5] M.N. B. Zhmud, L. Everlid, Gear design and tribology of EV transmissions, Proceedings of the Eighth European Conference and Exhibition on "Lubrication, Maintenance and Tribotechnology", LUBMAT, Preston, UK (17th - 19th July 2023).
[6] F. Mariño, J.M. Liñeira del Río, E.R. López, J. Fernández, Chemically modified nanomaterials as lubricant additive: time stability, friction, and wear, J. Mol. Liq. 382 (2023) 121913, https://doi.org/10.1016/j.molliq.2023.121913.
[7] A. Singh, N. Verma, T.G. Mamatha, A. Kumar, S. Singh, K. Kumar, Properties, functions and applications of commonly used lubricant additives: a review, Mater. Today Proc. 44 (2021) 5018–5022, https://doi.org/10.1016/j.matpr.2021.01.029.
[8] S. Wang, D. Chen, Q. Hong, Y. Gui, Y. Cao, G. Ren, Z. Liang, Surface functionalization of metal and metal oxide nanoparticles for dispersion and tribological applications – a review, J. Mol. Liq. 389 (2023) 122821, https://doi.org/10.1016/j.molliq.2023.122821.
[9] M. Gulzar, H.H. Masjuki, M.A. Kalam, M. Varman, N.W.M. Zulkifli, R.A. Mufti, R. Zahid, Tribological performance of nanoparticles as lubricating oil additives, J. Nanoparticle Res. 18 (2016) 223, https://doi.org/10.1007/s11051-016-3537-4.
[10] N.G. Demas, E.V. Timofeeva, J.L. Routbort, G.R. Fenske, Tribological effects of BN and MoS2 nanoparticles added to polyalphaolefin oil in piston skirt/cylinder liner tests, Tribol. Lett. 47 (2012) 91–102, https://doi.org/10.1007/s11249-012-9965-0.
[11] D. Berman, L.I. Farfan-Cabrera, A. Rosenkranz, A. Erdemir, 2D materials for durable and sustainable electric vehicles, Nat. Rev. Mater. 9 (2024) 527–529, https://doi.org/10.1038/s41578-024-00680-3.
[12] D. Berman, L.I. Farfan-Cabrera, A. Rosenkranz, A. Erdemir, Advancing the frontiers of EV tribology with 2D materials – a critical perspective, Mater. Sci. Eng. R Rep. 161 (2024) 100855, https://doi.org/10.1016/j.mser.2024.100855.
[13] X. Zhang, T. Ren, Z. Li, Recent advances of two-dimensional lubricating materials: from tunable tribological properties to applications, J. Mater. Chem. A 11 (2023) 9239–9269, https://doi.org/10.1039/D2TA08489A.
[14] H.A. Zaharin, M.J. Ghazali, N. Thachnatharen, F. Ezzah, R. Walvekar, M. Khalid, Progress in 2D materials based Nanolubricants: a review, FlatChem 38 (2023) 100485, https://doi.org/10.1016/j.flatc.2023.100485.
[15] J. Swapnalin, B. Koneru, R. Boddula, D. Rangappa, P. Banerjee, 2D Nanomaterials as Lubricant Additives, 2023, pp. 97–112, https://doi.org/10.1016/B978-0-323-91759-9.00012-5.

[16] M. Marian, D. Berman, A. Rota, R.L. Jackson, A. Rosenkranz, Layered 2D nanomaterials to tailor friction and wear in machine elements, Rev. 9 (2022) 2101622, https://doi.org/10.1002/admi.202101622.
[17] M. Kamal Kamarulzaman, S. Hisham, K. Kadirgama, D. Ramasamy, M. Samykano, Z. Said, A.K. Pandey, Improvement in stability and thermophysical properties of CNC-MXene nanolubricant for Tribology application, J. Mol. Liq. 381 (2023) 121695, https://doi.org/10.1016/j.molliq.2023.121695.
[18] A. Rosenkranz, M.C. Righi, A.V. Sumant, B. Anasori, V.N. Mochalin, Perspectives of 2D MXene, Tribology 35 (2023) 2207757, https://doi.org/10.1002/adma.202207757.
[19] J. Yang, B. Chen, H. Song, H. Tang, C. Li, Synthesis, Characterization, and Tribological Properties of Two-Dimensional Ti3C2, vol. 49, 2014, pp. 926–932, https://doi.org/10.1002/crat.201400268.
[20] X. Zhang, M. Xue, X. Yang, Z. Wang, G. Luo, Z. Huang, X. Sui, C. Li, Preparation and tribological properties of Ti3C2(OH)2 nanosheets as additives in base oil, RSC Adv. 5 (2015) 2762–2767, https://doi.org/10.1039/c4ra13800g.
[21] Y. Liu, X. Zhang, S. Dong, Z. Ye, Y. Wei, Synthesis and tribological property of Ti3C2TX nanosheets, J. Mater. Sci. 52 (2017) 2200–2209, https://doi.org/10.1007/s10853-016-0509-0.
[22] X. Lu, X. Gu, Y. Shi, A review on the synthesis of MXenes and their lubrication performance and mechanisms, Tribol. Int. 179 (2023) 108170, https://doi.org/10.1016/j.triboint.2022.108170.
[23] G. Boidi, J.C.F. de Queiróz, F.J. Profito, A. Rosenkranz, Ti3C2Tx MXene nanosheets as lubricant additives to lower friction under high loads, sliding ratios, and elevated temperatures, ACS Appl. Nano Mater. 6 (2023) 729–737, https://doi.org/10.1021/acsanm.2c05033.
[24] W. Ma, T. Li, W. Li, H. Tang, L. Zhang, Y. Yu, Z. Qiao, Ti3C2Tx MXenes – an effective and long-storable oil lubricant additive, Tribol. Int. 180 (2023) 108273, https://doi.org/10.1016/j.triboint.2023.108273.
[25] Y. Cui, S. Xue, Z. Liu, T. Wang, S. Liu, Q. Ye, F. Zhou, W. Liu, Synergistic effect of MXene and PTFE with multi-structure as lubricant additives for tribological applications, Carbon 220 (2024) 118896, https://doi.org/10.1016/j.carbon.2024.118896.
[26] J. Gao, C.-F. Du, T. Zhang, X. Zhang, Q. Ye, S. Liu, W. Liu, Dialkyl dithiophosphate-functionalized Ti3C2Tx MXene nanosheets as effective lubricant additives for antiwear and friction reduction, ACS Appl. Nano Mater. 4 (2021) 11080–11087, https://doi.org/10.1021/acsanm.1c02556.
[27] Commission Decision (EU) 2018/1702 of 8 November 2018 establishing the EU Ecolabel criteria for lubricants (notified under document C(2018) 7125). https://eur-lex.europa.eu/eli/dec/2018/1702/oj. (Accessed 27 September 2023).
[28] M. Zhang, X. Wang, X. Fu, Performance and anti-wear mechanism of CaCO 3 nanoparticles as a green additive in poly-alpha-olefin, Tribol. Int. 42 (2009) 1029–1039, https://doi.org/10.1016/j.triboint.2009.02.012.
[29] Q. Sunqing, D. Junxiu, C. Guoxu, Wear and Friction Behaviour of CaCO3 Nanoparticles Used as Additives in Lubricating Oils, vol. 12, 2000, pp. 205–212, https://doi.org/10.1002/ls.3010120207.
[30] T. Kulkarni, B. Toksha, A. Chatterjee, J. Naik, A. Autee, Anti-wear (AW) and extreme-pressure (EP) behavior of jojoba oil dispersed with green additive CaCO3 nanoparticles, J. Eng. Appl. Sci. 70 (2023) 29, https://doi.org/10.1186/s44147-023-00202-y.
[31] K. Vyavhare, R.B. Timmons, A. Erdemir, P.B. Aswath, Tribological interaction of plasma-functionalized CaCO3 nanoparticles with zinc and ashless dithiophosphate additives, Tribol. Lett. 69 (2021) 49, https://doi.org/10.1007/s11249-021-01423-z.
[32] J.M. Liñeira del Río, F. Mariño, E.R. López, D.E.P. Gonçalves, J.H.O. Seabra, J. Fernández, Tribological enhancement of potential electric vehicle lubricants using coated TiO2 nanoparticles as additives, J. Mol. Liq. 371 (2023) 121097, https://doi.org/10.1016/j.molliq.2022.121097.
[33] R. Babou Kammoe, S. Hamoudi, F. Larachi, K. Belkacemi, Synthesis of CaCO3 nanoparticles by controlled precipitation of saturated carbonate and calcium nitrate aqueous solutions, Can. J. Chem. Eng. 90 (2012), https://doi.org/10.1002/cjce.20673.
[34] Y. Wang, W. Eli, L. Zhang, H. Gao, Y. Liu, P. Li, A new method for surface modification of nano-CaCO3 and nano-Al2O3 at room temperature, Adv. Powder Technol. 21 (2010) 203–205, https://doi.org/10.1016/j.apt.2009.12.006.
[35] H. Zaharin, M. Ghazali, M. Khalid, T. Nagarajan, W. Pin, F. Ezzah, G. Ong, R. W, A. Rasheed, Tribological, oxidation and thermal analysis of advanced microwave–hydrothermal synthesised Ti3C2Tx MXene as additives in outboard engine oil, Lubricants 11 (2023) 264, https://doi.org/10.3390/lubricants11060264.
[36] K.I. Nasser, J.M. Liñeira del Río, E.R. López, J. Fernández, Synergistic effects of hexagonal boron nitride nanoparticles and phosphonium ionic liquids as hybrid lubricant additives, J. Mol. Liq. 311 (2020) 113343, https://doi.org/10.1016/j.molliq.2020.113343.
[37] N.U. Kiran, A.B. Deore, M.A. More, D.J. Late, C.S. Rout, P. Mane, B. Chakraborty, L. Besra, S. Chatterjee, Comparative study of cold electron emission from 2D Ti3C2TX MXene nanosheets with respect to its precursor Ti3SiC2 MAX phase, ACS Appl. Electron. Mater. 4 (2022) 2656–2666, https://doi.org/10.1021/acsaelm.2c00128.
[38] V.H.J.M.d. Santos, D. Pontin, G.G.D. Ponzi, A.S.d.G.e. Stepanha, R.B. Martel, M. K. Schütz, S.M.O. Einloft, F. Dalla Vecchia, Application of Fourier Transform infrared spectroscopy (FTIR) coupled with multivariate regression for calcium carbonate (CaCO3) quantification in cement, Constr. Build. Mater. 313 (2021) 125413, https://doi.org/10.1016/j.conbuildmat.2021.125413.
[39] B. Shentu, J. Li, Z. Weng, Effect of oleic acid-modified nano-CaCO3 on the crystallization behavior and mechanical properties of polypropylene, Chin. J. Chem. Eng. 14 (2006) 814–818, https://doi.org/10.1016/S1004-9541(07)60018-4.
[40] A. Iqbal, N. Hamdan, Investigation and optimization of mxene functionalized mesoporous titania films as efficient photoelectrodes, Materials 14 (2021) 6292, https://doi.org/10.3390/ma14216292.
[41] A.A. Emerenciano, R.M. do Nascimento, A.P.C. Barbosa, K. Ran, W.A. Meulenberg, J. Gonzalez-Julian, Ti3C2 MXene membranes for gas separation: influence of heat treatment conditions on D-spacing and surface, Functionalization 12 (2022) 1025, https://doi.org/10.3390/membranes12101025.
[42] P. Tandon, G. Förster, R. Neubert, S. Wartewig, Phase transitions in oleic acid as studied by X-ray diffraction and FT-Raman spectroscopy, J. Mol. Struct. 524 (2000) 201–215, https://doi.org/10.1016/S0022-2860(00)00378-1.
[43] S. Deepika, K. Hait, Y. Chen, Optimization of milling parameters on the synthesis of stearic acid coated CaCO3 nanoparticles, J. Coating Technol. Res. 11 (2014) 273–282, https://doi.org/10.1007/s11998-013-9547-6.
[44] X. Li, G. Fan, C. Zeng, Synthesis of ruthenium nanoparticles deposited on graphene-like transition metal carbide as an effective catalyst for the hydrolysis of sodium borohydride, Int. J. Hydrogen Energy 39 (2014) 14927–14934, https://doi.org/10.1016/j.ijhydene.2014.07.029.
[45] Y. Huang, H. Yang, Y. Zhang, Y. Zhang, Y. Wu, M. Tian, P. Chen, R. Trout, Y. Ma, T.-H. Wu, Y. Wu, N. Liu, A safe and fast-charging lithium-ion battery anode using MXene supported Li3VO4, J. Mater. Chem. A 7 (2019) 11250–11256, https://doi.org/10.1039/C9TA02037C.
[46] C.B. Cockreham, X. Zhang, H. Li, E. Hammond-Pereira, J. Sun, S.R. Saunders, Y. Wang, H. Xu, D. Wu, Inhibition of AlF3·3H2O impurity formation in Ti3C2Tx MXene synthesis under a unique CoFx/HCl etching environment, ACS Appl. Energy Mater. 2 (2019) 8145–8152, https://doi.org/10.1021/acsaem.9b01618.
[47] M. Kati, Behaviour of radio-thermoluminescence (X-Ray irradiated), thermal and structural characterization of limestone, Celal Bayar Üniversitesi Fen Bilimleri Dergisi 18 (2022) 435–441, https://doi.org/10.18466/cbayarfbe.1106810.
[48] J. Kim, S.K. Bea, Y.H. Kim, D.-W. Kim, K.-Y. Lee, C.-M. Lee, Improved suspension stability of calcium carbonate nanoparticles by surface modification with oleic acid and phospholipid, Biotechnol. Bioproc. Eng. 20 (2015) 794–799, https://doi.org/10.1007/s12257-014-0898-3.
[49] L.-H. Sun, Z.-G. Yang, X.-H. Li, Mechanical and Tribological Properties of Polyoxymethylene Modified with Nanoparticles and Solid Lubricants, vol. 48, 2008, pp. 1824–1832, https://doi.org/10.1002/pen.21150.
[50] J.M. Liñeira del Río, G. Alonso Pérez, A. Martínez, D. Peña, J. Fernández, Tribological improvement of potential lubricants for electric vehicles using double functionalized graphene oxide as additives, Tribol. Int. 193 (2024) 109402, https://doi.org/10.1016/j.triboint.2024.109402.
[51] J.M. Liñeira del Río, A. Alba, M.J.G. Guimarey, J.I. Prado, A. Amigo, J. Fernández, Surface tension, wettability and tribological properties of a low viscosity oil using CaCO3 and CeF3 nanoparticles as additives, J. Mol. Liq. 391 (2023) 123188, https://doi.org/10.1016/j.molliq.2023.123188.
[52] S. Yi, J. Li, Y. Liu, X. Ge, J. Zhang, J. Luo, In-situ formation of tribofilm with Ti3C2Tx MXene nanoflakes triggers macroscale superlubricity, Tribol. Int. 154 (2021) 106695, https://doi.org/10.1016/j.triboint.2020.106695.
[53] S. Yi, Y. Guo, J. Li, Y. Zhang, A. Zhou, J. Luo, Two-dimensional molybdenum carbide (MXene) as an efficient nanoadditive for achieving superlubricity under ultrahigh pressure, Friction 11 (2023) 369–382, https://doi.org/10.1007/s40544-022-0597-6.
[54] A.K. Sharma, A.K. Tiwari, A.R. Dixit, Mechanism of nanoparticles functioning and effects in machining processes: a review, Mater. Today Proc. 2 (2015) 3539–3544, https://doi.org/10.1016/j.matpr.2015.07.331.
[55] M. Zhang, X. Wang, X. Fu, Y. Xia, Performance and anti-wear mechanism of CaCO3 nanoparticles as a green additive in poly-alpha-olefin, Tribol. Int. 42 (2009) 1029–1039, https://doi.org/10.1016/j.triboint.2009.02.012.
[56] Y. Ren, X. Fan, P. Feng, J. Cao, M. Zhu, Ti3C2Tx quantum dots as high-performance additive in lubrication application, Tribol. Int. 189 (2023) 108938, https://doi.org/10.1016/j.triboint.2023.108938.
[57] C. Gu, Q. Li, Z. Gu, G. Zhu, Study on application of CeO2 and CaCO3 nanoparticles in lubricating oils, J. Rare Earths 26 (2008) 163–167, https://doi.org/10.1016/S1002-0721(08)60058-7.